Smartphone Battery Remaining Runtime Prediction Model Based on Particle Filtering and Monte Carlo Simulation

Kaili Zhou *, Shiya Huang, Ran Ling

Information Science and Technology College, Dalian Maritime University, Dalian, China

* Corresponding Author Email: zhoukaili@dlmu.edu.cn

Abstract. This paper proposes a closed-loop electro-thermal coupling modeling method for predicting the remaining battery life of smartphones. The method maps the screen, processor, network, GPS, and background tasks to system power consumption, and combines a second-order Thevenin equivalent circuit, dynamic SOC updates, effective capacity correction, and a first-order thermal model to characterize the feedback relationships among power consumption, current, voltage, temperature, and capacity degradation. Building on this foundation, a particle filter is introduced to perform individualized calibration of key parameters, a semi-Markov process is used to generate typical load sequences, and Monte Carlo simulations are employed to obtain the TTE distribution, confidence intervals, and the risk of premature shutdown. Validation results indicate that the model can adapt to different loads, temperatures, and battery aging states, providing a universally applicable modeling framework for battery state assessment and runtime prediction in mobile devices.

Keywords: Monte Carlo Simulation, Semi-Markov Process, Second-Order Thevenin Model.

1. Introduction

During continuous operation, the battery state of a mobile device is jointly affected by load variations, temperature fluctuations, and component aging. Traditional battery life estimates rely primarily on the remaining charge percentage or simple power consumption extrapolation, which struggle to account for nonlinear changes caused by voltage drop, thermal effects, and high-load switching [1]. This approach is particularly prone to significant deviations in scenarios involving low battery levels, low temperatures, or high power consumption. To enhance the stability and applicability of predictions, this paper constructs a closed-loop electro-thermal coupling algorithm framework that integrates system power consumption, battery circuit response, temperature evolution, and capacity degradation into a unified computational workflow [2]. The framework employs a second-order Thevenin equivalent circuit to describe terminal voltage dynamics, uses effective capacity correction to account for the effects of aging and discharge rates, and incorporates a first-order thermal model to establish a feedback relationship between temperature and internal resistance. At the prediction level, particle filtering is used for online calibration of key parameters, and the remaining usage time distribution is obtained through scenario-driven load generation and Monte Carlo simulation [3]. Applying this method to the discharge process of a smartphone, it enables unified modeling across scenarios such as standby, video playback, navigation, gaming, and low-temperature conditions, providing a transferable model framework for predicting the battery life of end devices and assessing battery health.

2. Closed-Loop Electro-Thermal Battery Discharge Model

To describe the battery discharge process of smartphones under dynamic usage scenarios, a closed-loop discharge model coupling electrical, thermal, and load behaviors is constructed. Driven by system power demand, the model places user behavior, battery electrical response, and temperature variation within the same computational framework to characterize the continuous evolution of battery states over time.

On the load side, subsystem activities such as the screen, processor, network, GPS, and background tasks do not directly affect SOC. Instead, they are first converted into power demand and then influence the discharge process. Therefore, a mapping from utilization to power consumption is established, converting various behavioral features into the total power demand $P_{\text{sys}}(t)$. On the electrical side, the equivalent circuit model calculates the terminal voltage $V(t)$ and discharge current $I(t)$ according to the power demand, which then drives the update of SOC.

Changes in SOC further affect the open-circuit voltage and terminal voltage, while the terminal voltage determines the current required to maintain the same power demand. As a result, closed-loop feedback is formed between $I(t)$ and $V(t)$. The discharge current is no longer a predefined external input but is dynamically determined by the system state.

The thermal behavior is described using a first-order lumped-parameter thermal model. Temperature variation affects internal resistance and effective capacity, which in turn changes the terminal voltage and the decay rate of SOC. At the same time, changes in current alter the level of Joule heat generation and affect the temperature at the next time step. Electrical feedback and thermal feedback together form the closed-loop mechanism, allowing the model to describe the coupled evolution of power consumption, current, voltage, temperature, and SOC.

2.1. Power Demand Modeling

Let $U_i(t)$ denote the utilization of subsystem i at time t, including factors such as screen brightness, processor workload, network activity, GPS usage, and background tasks. Following measurement-driven power modeling approaches, the total power consumption is expressed as

$$P_{\text{sys}}(t) = P_{\text{idle}} + C_{\text{scre}}U_{\text{scre}}(t) + C_{\text{proc}}U_{\text{proc}}(t) + C_{\text{net}}U_{\text{net}}(t) + C_{\text{gps}}U_{\text{gps}}(t) + C_{\text{oth}}U_{\text{oth}}(t) \tag{1}$$

where P_{idle} represents the baseline system power consumption, and the coefficients describe the contribution of different subsystem activities to power consumption. During a discharge cycle, these parameters are assumed to remain approximately constant, while differences between usage scenarios are mainly reflected by variations in the utilization signals $U_i(t)$.

For screen power consumption, the screen-on state and brightness level are represented by $U_{\text{scre}}(t)$, while hardware differences such as device size are absorbed into C_{scre}. Network power consumption is affected by signal strength and transmission rate, but the network environment is assumed to be relatively stable during model development, so C_{net} is treated as a fixed parameter. Repetitive activities that cannot be separated individually are included in the background power term $C_{\text{oth}}U_{\text{oth}}(t)$ to maintain a complete decomposition of power consumption.

2.2. Power-to-Current Coupling

Over a short time scale, the system power consumption is assumed to remain constant. Under this assumption, the discharge current satisfies $I(t) = P_{\text{sys}}(t) / V(t)$.

This relationship establishes a direct connection between power demand and the electrical state of the battery. As the discharge process continues, the terminal voltage gradually decreases. To maintain the same power level, the battery must supply a higher discharge current. The increase in current leads to greater ohmic losses, which further reduce the terminal voltage, forming a feedback coupling between voltage and current.

This behavior becomes more pronounced under low-SOC and high-load conditions. As the voltage margin continues to shrink, the system becomes increasingly sensitive to current variations. As a result, accelerated battery depletion and a rapid reduction in remaining runtime are often observed during the later stage of discharge.

2.3. SOC Dynamics with Aging-Aware Effective Capacity

In the closed-loop discharge model, $SOC(t)$ is used to represent the remaining battery charge state. To capture the effects of aging, temperature conditions, and discharge rate on the discharge process, an effective capacity term $Q_{\text{eff}}(t)$ is introduced. Let $SOC(t) \in [0,1]$. Based on the Coulomb counting principle, the continuous evolution of SOC can be written as

$$\frac{dSOC(t)}{dt} = -\frac{I(t)}{3600 Q_{\text{eff}}(t)} \tag{2}$$

where $I(t)$ is the discharge current (A), $Q_{\text{eff}}(t)$ is the effective capacity (Ah), and the factor 3600 is used for time unit conversion.

Substituting the power model and the power-to-current coupling relationship yields the power-driven SOC update equation:

$$\frac{dSOC(t)}{dt} = -\frac{P_{\text{sys}}(t)}{3600 Q_{\text{eff}}(t) V(t)} \tag{3}$$

It can be seen that the SOC decay rate is jointly affected by system power consumption and terminal voltage. An increase in power demand or a decrease in terminal voltage both accelerate energy consumption over time. The rapid battery drain commonly observed under high-load and low-battery conditions is essentially a result of this coupling effect.

The effective capacity is defined as $Q_{\text{eff}}(t) = Q_{\text{rated}} f_{\text{deg}}(t) f_T(T(t)) f_C(I(t))$, where Q_{rated} is the rated capacity, and $f_{\text{deg}}(t)$, $f_T(T(t))$, and $f_C(I(t))$ represent correction factors associated with aging, temperature, and current rate, respectively. With these correction terms, the available capacity is no longer treated as a fixed constant but varies dynamically with the operating state of the battery.

For aging effects, a normalized multiplicative correction is adopted:

$$f_{\text{deg}}(t) = 1 - \delta \frac{t_{\text{cycle}}}{t_{\text{cycle,max}}} \left(1 + \gamma \frac{C_{\text{rate}}}{C_{\text{ref}}}\right) \left(1 + \lambda \frac{T(t) - T_{\text{ref}}}{T_{\max} - T_{\min}}\right) \tag{4}$$

where t_{cycle} denotes the cycle count and $t_{\text{cycle,max}}$ is the normalized lifetime scale; C_{rate} is the charging rate and C_{ref} is the reference rate. The parameters δ, γ, and λ control the contributions of baseline aging, rate-accelerated aging, and temperature-accelerated aging, respectively.

For the rate effect, a correction form similar to Peukert's law is adopted:

$$f_C(I(t)) = \alpha \left(\frac{I(t)}{I_{\text{ref}}}\right)^{-\beta}, \quad \alpha > 0, \beta > 0 \tag{5}$$

where I_{ref} is the reference current, and α and β are positive parameters. As the discharge current increases, the available capacity decreases accordingly, reflecting the capacity loss observed under high-rate discharge conditions.

2.4. Electro-Thermal Coupling

Temperature mainly changes the discharge process through internal resistance and effective capacity [4]. The internal resistance of the battery increases with cycle count and is also affected by operating temperature. Therefore, the ohmic resistance is written as

$$R_0(T(t), t_{\text{cycle}}) = R_{0,\text{nom}} \left(1 + \alpha_R \,|T(t) - T_{\text{ref}}|\right)\left(1 + \beta_R t_{\text{cycle}}\right) \tag{6}$$

where $R_{0,\text{nom}}$ is the nominal internal resistance at the reference temperature, α_R describes the change in internal resistance caused by temperature deviation, and β_R describes the increase in internal resistance caused by cycling aging. With this expression, long-term aging and electro-thermal changes during short-term discharge can be linked through R_0.

Irreversible heat generation is approximated by Joule heat: $Q_{\text{gen}}(t) \approx I^2(t)R_0(T(t), t_{\text{cycle}})$.

When the load increases, the discharge current $I(t)$ rises, and the heat generation $Q_{\text{gen}}(t)$ also increases. If the battery has already aged noticeably, or if the temperature condition further increases the internal resistance, both heat generation and voltage loss under the same current become more evident.

Since smartphone logs usually provide only device-level temperature and cannot easily give the multi-point temperature distribution inside the cell, a first-order lumped-parameter thermal model is used to describe temperature evolution:

$$C_{\text{th}} \frac{dT(t)}{dt} = \frac{T_{\text{amb}} - T(t)}{R_{\text{th}}} + Q_{\text{gen}}(t) \tag{7}$$

where T_{amb} is the ambient temperature, and C_{th} and R_{th} denote the equivalent thermal capacitance and thermal resistance, respectively. This model keeps the main features of temperature rise and thermal stabilization, while avoiding excessive modeling of the unobservable internal temperature field.

In the closed-loop model, temperature is not a standalone output state. An increase in temperature changes R_0, which then affects the terminal voltage and discharge current. Changes in current further alter the heat generation level at the next time step. This feedback relationship can explain the accelerated discharge accompanied by temperature rise under high-load scenarios.

2.5. Second-Order Thevenin Equivalent Circuit Model

To describe the transient response and slow recovery process of terminal voltage during load switching, a second-order Thevenin equivalent circuit model is used, as shown in Fig. 1. The model contains two polarization branches and can capture the voltage lag caused by frequent load changes during smartphone operation.

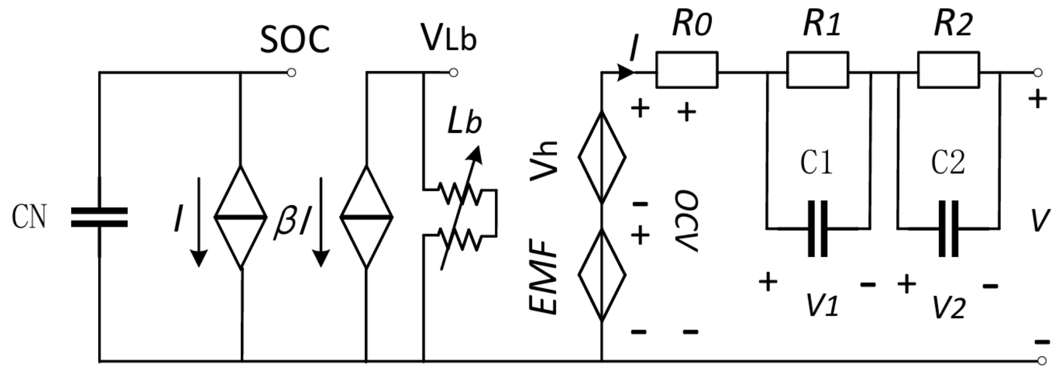

Fig. 1 Second-order Thevenin equivalent circuit model (2RC)

Let the two polarization voltages be $V_1(t)$ and $V_2(t)$. Their dynamics are written as

$$\frac{dV_1(t)}{dt} = -\frac{V_1(t)}{R_1C_1} + \frac{I(t)}{C_1}, \quad \frac{dV_2(t)}{dt} = -\frac{V_2(t)}{R_2C_2} + \frac{I(t)}{C_2} \tag{8}$$

The terminal voltage is calculated as

$$V(t) = OCV(SOC(t), T(t)) - I(t)R_0(T(t), t_{\text{cycle}}) - V_1(t) - V_2(t) \tag{9}$$

where $V(t)$ is the terminal voltage variable used throughout the closed-loop model. It is involved in power-to-current conversion, SOC update, and cutoff judgment, and is the key variable connecting power demand, battery state, and shutdown conditions.

2.6. OCV Parameterization

The relationship between open-circuit voltage OCV and SOC is clearly nonlinear. To make continuous-time simulation easier to call, OCV is parameterized using a polynomial form, and the coefficients are fitted based on the public OCV test data from CALCE:

$$OCV(SOC) = \sum_{m=0}^{M} \alpha_m SOC^m \tag{10}$$

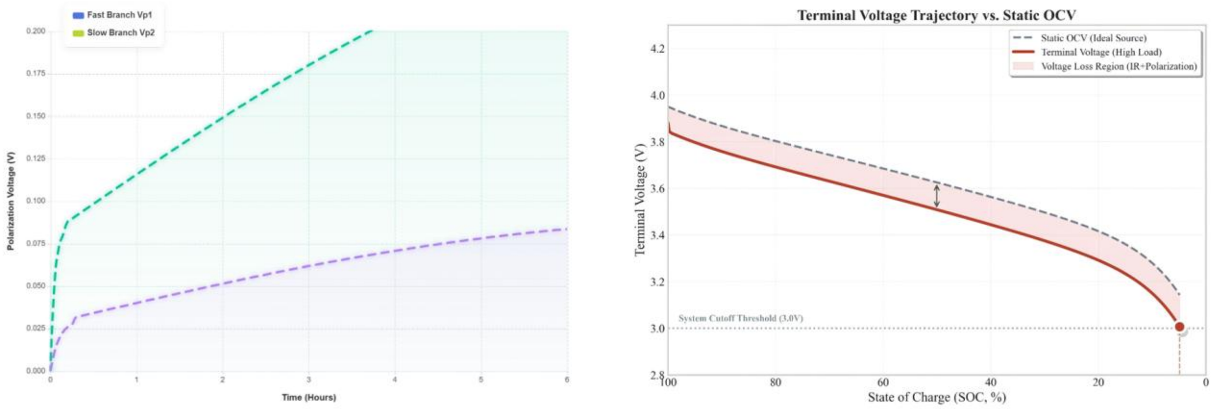

(a) Second-Order Polarization Dynamics (b) Terminal Voltage Trajectory vs. Static OCV

Fig. 2 Second-order polarization dynamics and terminal voltage trajectory relative to static OCV

Fig.2(a) shows the two polarization components in the second-order RC model. The fast component V_{p1} mainly corresponds to activation polarization and responds quickly to current changes. The slow component V_{p2} mainly corresponds to concentration polarization, changes more gradually, and has a time constant of about $\tau_2 \approx 38\,\text{s}$. The two time scales together explain the voltage recovery process after a sudden load change. After a high-power operation ends, the terminal voltage does not immediately return to the static OCV, but instead goes through a slow rebound stage.

Fig. 2(b) compares the static open-circuit voltage with the terminal voltage under load. Under high-load conditions, the terminal voltage remains lower than the static OCV, and the difference mainly comes from ohmic resistance loss and polarization voltage. When 3.0 V is used as the cutoff voltage, the terminal voltage may trigger shutdown while SOC is still about 12%. This shows that phone shutdown is not always caused by complete battery depletion. Voltage collapse caused by high current may also trigger cutoff earlier. The remaining energy that cannot continue to be released can be viewed as stranded energy, which explains the "battery suddenly becomes less durable" phenomenon under low-temperature or high-load scenarios such as gaming.

2.7. Data Sources and Parameter Calibration

Model parameters are mainly calibrated based on public datasets, so that each module has clear data support.

The NASA PCoE Li-ion Battery Aging Dataset provides voltage, current, and temperature sequences under different operating conditions, which are used to calibrate the parameters of the equivalent circuit model and the thermal model. The SherLock smartphone telemetry dataset records long-term smartphone operation logs, including screen, CPU, network, and background activity information. Based on these records, the mapping between utilization and power consumption $P_{sys}(t)$ is established.

The parameters related to capacity degradation and internal resistance growth are taken with reference to the Comprehensive Battery Aging Dataset and the Lithium-Ion Battery Aging Study. These two datasets cover aging processes under different temperatures, rates, and cycling conditions, and can provide reasonable parameter ranges and calibration bases for the aging factor $f_{\deg}(t)$ and the internal resistance model $R_0(T(t), t_{\text{cycle}})$.

By assigning different data sources to the power, electrical, thermal, and aging modules, the model parameters can retain consistent physical meanings.

3. Time-to-Empty Prediction under Usage Scenarios

After the closed-loop discharge model is obtained, it is further used to predict the remaining usage time of smartphones. Time-to-Empty (TTE) is treated as a random variable rather than a single deterministic value. In addition to the typical battery life P50, the prediction also provides the uncertainty interval P5-P95 and the risk of early shutdown, which are used to describe the spread of future battery life performance.

The uncertainty mainly comes from two aspects. On the one hand, different devices vary in battery health, internal resistance level, and power consumption characteristics. On the other hand, future usage behavior itself is random, since users may switch between standby, video playback, navigation, gaming, and other states. Therefore, TTE prediction needs to consider both the uncertainty of device parameters and the effects brought by future load changes.

3.1. Cutoff-Based TTE Definition and Parameter Personalization

Given the terminal voltage $V(t)$, state of charge $SOC(t)$, and temperature $T(t)$ output by the closed-loop model, the shutdown time is defined using a cutoff voltage rule:

$$t_{\text{shut}} = \inf\left\{t \ge 0 \mid V(t) \le V_{\text{cutoff}}\right\}, \quad TTE = t_{\text{shut}} \tag{11}$$

Compared with estimating remaining battery life only based on SOC, this definition better matches the actual operating mechanism of smartphones. Under high-load conditions or when the load fluctuates strongly, the terminal voltage may reach the cutoff threshold earlier because of voltage sag, which then triggers shutdown. Therefore, TTE depends not only on the remaining charge but also on the dynamic change of the terminal voltage.

To reduce the bias caused by device differences and environmental differences, particle filtering is used to personalize key parameters. Within a short observation window, particle filtering propagates parameter particles and updates their weights based on the observed voltage, current, and temperature sequences, thereby obtaining the posterior parameter distribution matched to the current device state.

The calibrated parameter set is defined as $\theta = \left\{C_{\text{idle}}, C_{\text{scre}}, C_{\text{proc}}, C_{\text{net}}, C_{\text{gps}}, Q_{\text{eff},0}, R_0, f_{\deg}\right\}$, where C_{idle}, C_{scre}, C_{proc}, C_{net}, and C_{gps} denote the weights of different power consumption channels, $Q_{\text{eff},0}$ is the initial effective capacity, R_0 denotes the ohmic internal resistance, and $f_{\deg}$ is the aging factor that is approximately constant during the current discharge stage.

After calibration, the model can correct the power consumption characteristics and battery state estimates based on observed data, making later predictions closer to the actual operation of the device. Factors such as network condition changes, screen usage intensity, and battery aging level can also be separated during the parameter update process, which improves the credibility of TTE prediction.

3.2. Scenario-Driven Monte Carlo Simulation

To represent the uncertainty of future user behavior, six typical usage scenarios are defined, and a semi-Markov process is used to generate future load sequences [5]. The six scenarios are defined as follows: S_1 represents standby at room temperature, S_2 represents light usage, S_3 represents video playback, S_4 represents navigation, S_5 represents high-load gaming, and S_6 represents standby under low-temperature conditions. Among them, S_1 - S_5 mainly correspond to power consumption channels associated with the screen, computation, network, positioning, and background tasks, while S_6 is used to characterize the impact of low temperature on available capacity and voltage margin.

In each Monte Carlo simulation, the parameter vector $\theta^{(i)}$ is sampled from the posterior distribution obtained through particle filtering. A semi-Markov process is then used to generate the usage state sequence $S^{(i)}(t)$ and the corresponding load input $U^{(i)}(t)$. The closed-loop model is subsequently executed to obtain $V(t)$, $SOC(t)$, and $T(t)$, and $TTE^{(i)} = \inf\{t \ge 0 | \ V(t) \le V_{\text{cutoff}}\}$ is computed.

After N repeated simulations, an empirical distribution of TTE is obtained. Based on this distribution, the P50 value, the P5-P95 interval, and the risk of early shutdown are calculated.

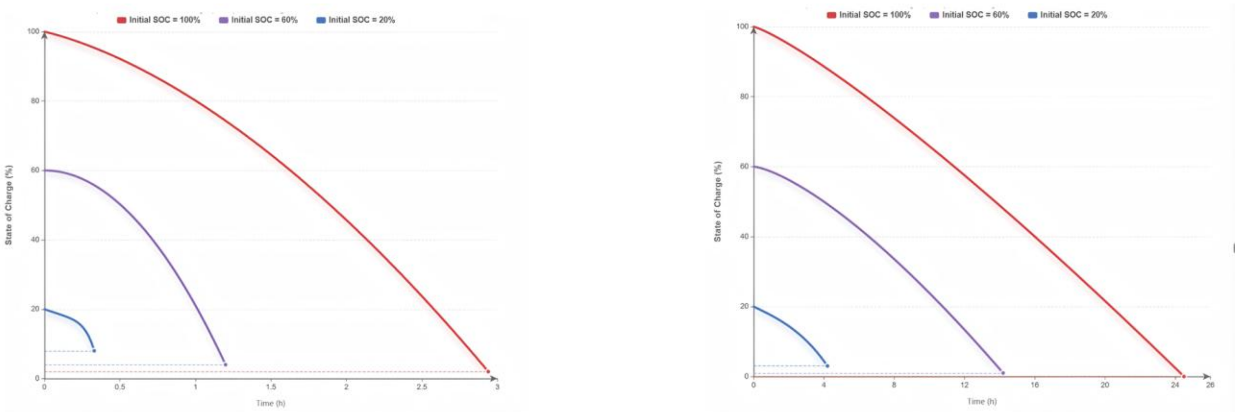

(a) High-load scenario (e.g., gaming) (b) Low-load scenario (e.g., idle/ligh use)

Fig. 3 SOC trajectories under different initial SOC values (100%, 60%, 20%) for representative high-load and low-load regimes

Fig. 3 shows discharge trajectories under different initial SOC levels. Under high-load conditions, lower initial SOC leads to a faster decline, and the slope continues to increase during the low-battery stage. This occurs because, as the terminal voltage decreases, a larger current is required to maintain the same power demand, which further increases internal resistance losses and polarization effects. The same trend appears under low-load conditions, but the magnitude is much smaller because current peaks are lower and the voltage margin is larger. Therefore, a low initial battery level amplifies the rapid power depletion observed under high load and increases the likelihood of an early cutoff triggered by the terminal voltage.

3.3. Validation on GreenHub Discharge Logs

To evaluate model performance on real smartphone usage data, GreenHub logs are used for validation. The raw records include battery voltage, temperature, battery level, charging status, screen status, application activity, and network-related metrics. During preprocessing, the logs are resampled to a 60 s grid. Only non-charging and monotonically discharging segments are retained, transition intervals near power connection or disconnection events are removed, and windows with a high missing-data rate are excluded.

Predictions are compared point-by-point with the observed battery level. Evaluation metrics include MAE, RMSE, P5-P95 coverage, and typical TTE prediction error. These metrics are used to assess trajectory fitting accuracy, uncertainty interval reliability, and remaining-time estimation error, respectively.

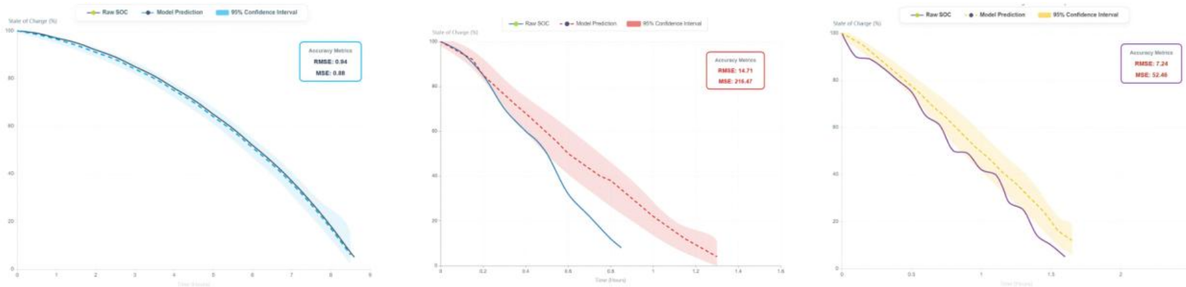

(a) Well-matched case (b) Severe aging + gaming (c) Cold + high load

Fig. 4 Predicted versus observed SOC examples on GreenHub discharge segments under different operating regimes

Fig. 4 presents three representative validation examples. In Fig. 4(a), the predicted trajectory almost overlaps with the observed SOC, and the uncertainty interval remains narrow, indicating that the model can capture the battery depletion trend well under normal discharge conditions. The corresponding results are RMSE=0.94 and MSE=0.88. Fig. 4(b) corresponds to a severe aging condition combined with gaming load. A persistent deviation appears after the initial stage of discharge, with RMSE=14.71 and MSE=216.47. This suggests that under high load and poor battery health, the effective capacity and internal resistance estimated from short observation segments may still be insufficient to fully describe the actual degradation level. Fig. 4(c) represents a low-temperature condition combined with high load. The error is smaller than that of the severe aging case, but the step-like decline remains noticeable, with RMSE=7.24 and MSE=52.46. This behavior is usually caused by sudden high-current events, whose effects become more pronounced during the low-battery stage through voltage sag and polarization losses.

The validation results show that the model performs well on typical discharge segments. However, when severe aging, low temperature, and high load occur simultaneously, prediction errors increase noticeably. For practical deployment, battery health and terminal voltage response under extreme conditions still require more refined online estimation.

3.4. Driver Attribution of Power Consumption

The differences in TTE across scenarios do not only come from the remaining battery level, but are also closely related to the power consumption structure. To analyze the main sources of battery drain in each scenario, the total power consumption is decomposed into several channels, including the baseline system, screen, computation, network, GPS, and background tasks.

Fig. 5(a) shows the real-time power consumption composition under different scenarios. In the room-temperature standby scenario, power consumption mainly comes from the baseline system and background tasks. Under light usage, the screen gradually becomes the main source of power consumption. Video playback increases both network transmission and decoding computation loads. Although the navigation scenario includes GPS power consumption, screen display and map rendering still account for the main proportion. The gaming scenario shows the most noticeable computation load peaks, along with stronger current consumption and temperature accumulation.

Fig. 5(b) gives the overall proportion of each power consumption channel. Under low- to medium-load conditions, screen power consumption usually accounts for a large proportion. As the load intensity increases, the importance of the computation and network modules gradually rises, and they become the dominant factors in the gaming scenario. In comparison, GPS power consumption remains at a low level, so the overall power consumption of the navigation scenario is usually lower than that of video playback and gaming.

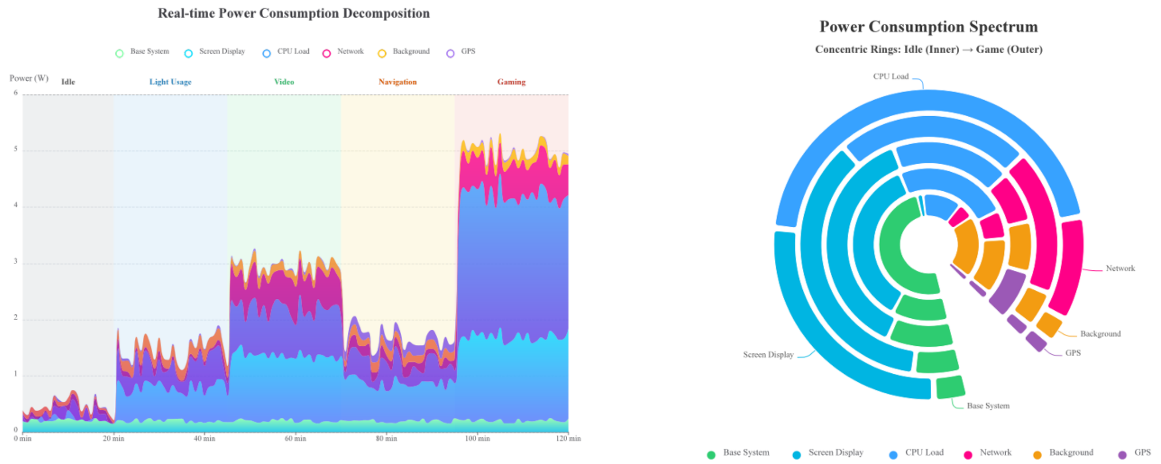

(a) Real-time stochastic power decomposition

(b) Power consumption spectrum across scenarios

Fig. 5 Power decomposition visualizations for driver attribution

In terms of battery life, the degree of TTE reduction roughly follows this order: high-load gaming, video playback, navigation, low-temperature standby, light usage, and room-temperature standby. Among them, gaming has the most obvious effect on TTE. High computation load not only increases the discharge current, but also strengthens internal resistance loss and heat accumulation at the same time. Video playback is jointly affected by continuous network transmission and decoding computation. Low-temperature standby does not greatly increase external power demand, but it reduces effective capacity and increases polarization loss, thereby shortening the available runtime.

Some factors have relatively limited effects in short-term prediction. For example, under stable room temperature and early-cycle conditions, charging rate, small temperature fluctuations, and minor changes in cycle count do not have a clear impact on a single discharge process. These factors are reflected more in long-term aging. Similarly, under high-load scenarios, even if GPS power consumption changes greatly in relative terms, its effect is easily masked by computation and network loads, making it difficult to noticeably change the typical TTE.

4. Compact Sensitivity Analysis

To evaluate the robustness of TTE prediction results, sensitivity analysis is conducted on the model structure, key parameters, and future usage variability. The evaluation metrics include the typical battery life TTE_{50}, the uncertainty width $\Delta_{90} = TTE_{95} - TTE_{5}$, and the risk probability $\mathrm{R}(T_0) = \mathrm{P}(TTE < T_0)$.

Structural sensitivity is assessed through ablation experiments. In each experiment, one model component is removed or replaced, and the shift in average TTE relative to the baseline model is calculated as $\Delta\mu = \mu_{\text{ablated}} - \mu_{\text{base}}$.

The ablation results show that replacing the 2RC structure with a 1RC structure causes the largest prediction drift. In smartphone scenarios with frequent load changes, both fast and slow polarization processes affect the cutoff time, so the second-order RC structure should not be simplified directly. Removing the thermal coupling also leads to a noticeable TTE bias because temperature changes the degree of voltage sag through R_0, which then affects the shutdown time. These results indicate that circuit polarization and thermal feedback are among the most sensitive structural components of the model.

Parameter sensitivity is analyzed using both Morris screening and Sobol indices. The Morris method is used to rank parameter importance, while Sobol indices distinguish between main effects and interaction effects [6].

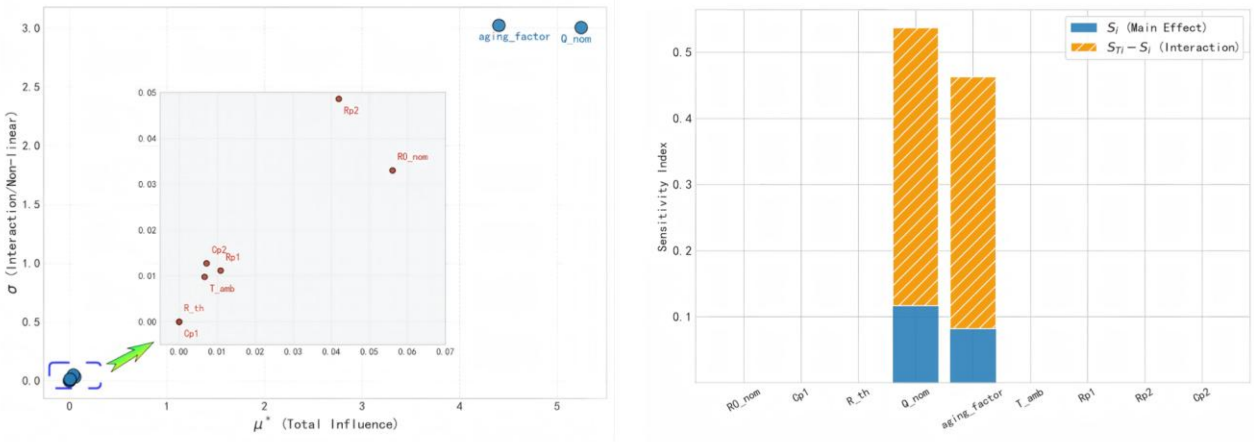

(a) Morris screening (b) Sobol indices

Fig. 6 Global parameter sensitivity results

The Morris results in Fig 6(a) show that Q_{nom} and f_{deg} lie in the high-impact region, indicating that parameters related to capacity and battery health contribute most strongly to TTE. At the same time, both parameters have relatively high σ values, suggesting nonlinear coupling with other parameters. In contrast, RC-related parameters such as $R_{0,\text{nom}}$, R_{p1}, and C_{p1} have smaller μ^* values. Changing these parameters individually has only a limited effect on TTE during short-term discharge prediction.

The Sobol results in Fig. 6(b) lead to a similar conclusion. The main effects of Q_{nom} and f_{deg} account for most of the variance, while the main effects of many circuit-level parameters are close to zero. However, some parameters still contribute through interaction terms. For example, R_{th} is not one of the strongest factors by itself, but under high-load conditions it interacts with R_0 and current-related losses to influence temperature evolution, which then affects the terminal voltage. In other words, available capacity determines the overall battery-life scale, while thermal and circuit parameters mainly modify the prediction error under specific load conditions.

The randomness of future user behavior also affects the prediction distribution. The results indicate that changing only the duration of a user's stay in a given state has a relatively limited effect on TTE_{50}. In contrast, increasing the probability of entering high-power states noticeably shortens TTE and widens the P5-P95 interval. When high-load states occur more frequently, the average power consumption rate increases, the terminal voltage approaches the cutoff threshold more easily, and tail risk rises accordingly.

Overall, TTE prediction is relatively sensitive to the 2RC polarization structure and thermal coupling. The parameters Q_{nom} and f_{deg} are the dominant factors affecting battery life, while for future user behavior, the probability of entering high-power states is more important than the duration of any individual state.

5. Conclusion

This paper constructs a model framework that combines electro-thermal coupling with scenario-driven analysis to predict smartphone battery life. The results show that the second-order RC structure and thermal feedback have a significant impact on terminal voltage changes during low-battery and high-load phases, and can explain phenomena such as premature shutdown and sudden drops in battery life. In validation using GreenHub logs, the predicted trajectories showed high consistency with observed SOC under typical discharge scenarios, with an RMSE as low as 0.94; however, when severe aging was combined with gaming loads, the error rose to 14.71, indicating that battery health remains a key factor affecting prediction accuracy. Sensitivity analysis further reveals that nominal capacity and the aging factor contribute most significantly to TTE; the probability of entering a high-power-consumption state will significantly shorten runtime and widen the uncertainty interval. Overall, this method enhances the interpretability and applicability of remaining time-to-exhaust (TTE) assessments under complex usage scenarios. Future research could further strengthen online parameter calibration under extreme operating conditions.

References

[1] Li Shuxian. A Study on SOC and SOT Estimation Based on a Temperature-Voltage-Heat Coupling Model for Lithium-Ion Batteries [D]. Chongqing University, 2019. DOI:10.27670/d.cnki.gcqdu.2019.002580.

[2] Yan Huixiang, Gan Xiaoyan, Wu Honghui, et al. Modeling and Simulation of Lithium-Ion Batteries Based on the Second-Order Thevenin Model [J]. Journal of Jiangsu University (Natural Science Edition), 2018, 39 (4): 403–408.

[3] Xie Yanxin, Wang Shunli, Shi Weihao, et al. A New Trace-Free Particle Filter Method for High-Fidelity SOC Estimation of Lithium-Ion Batteries [J]. Energy Storage Science and Technology, 2021, 10 (2): 722–731. DOI: 10.19799/j.cnki.2095-4239.2020.0357.

[4] Xie Jiale, Li Zengchao, Wang Guang, et al. A Model for Predicting Internal and External Temperatures of 18650 Lithium-Ion Batteries Based on Electrothermal Coupling Effects [J]. Journal of Mechanical Engineering, 2023, 59 (16): 342–352.

[5] Shangguan Danhua, Yan Weihua, Wei Junxia, et al. An Efficient Monte Carlo Simulation Method for Dynamic Transport Problems in Multiphysics Coupling Calculations [J]. Acta Physica Sinica, 2022, 71 (9): 16–22.

[6] Jin Mengxiao, Tian Yong, Michele Lancia, et al. Global Sensitivity Analysis of LID Facility Model Parameters Based on Morris, Sobol, and EFAST [J]. Chinese Journal of Rural Water and Hydropower, 2022, (6): 104–110.